


# Factors resisting protein adsorption on hydrophilic/hydrophobic self-assembled monolayers terminated with hydrophilic hydroxyl groups

Dangxin Mao(毛党新), Yuan-Yan Wu(吴园燕), Yusong Tu(涂育松)

**Citation:**Chin. Phys. B, 2024, 33 (**6**): 068701. DOI: 10.1088/1674-1056/ad39ca
Journal homepage: http://cpb.iphy.ac.cn; http://iopscience.iop.org/cpb

**What follows is a list of articles you may be interested in**

---

## Molecular dynamics simulations on the interactions between nucleic acids and a phospholipid bilayer

Yao Xu(徐耀), Shu-Wei Huang(黄舒伟), Hong-Ming Ding(丁泓铭), and Yu-Qiang Ma(马余强)
Chin. Phys. B, 2024, 33 (**2**): 028701. DOI: 10.1088/1674-1056/ad1178

## Unraveling the molecular mechanism of prion disease: Insights from $\alpha$2 area mutations in human prion protein

Rongri Tan(谈荣日), Kui Xia(夏奎), Damao Xun(寻大毛), Wenjun Zong(宗文军), and Yousheng Yu(余幼胜)
Chin. Phys. B, 2023, 32 (**12**): 128703. DOI: 10.1088/1674-1056/ad08a8

## Kinesin-microtubule interaction reveals the mechanism of kinesin-1 for discriminating the binding site on microtubule

Yi-Zhao Geng(耿轶钊), Li-Ai Lu(鲁丽爱), Ning Jia(贾宁), Bing-Bing Zhang(张冰冰), and Qing Ji(纪青)
Chin. Phys. B, 2023, 32 (**10**): 108701. DOI: 10.1088/1674-1056/acdfc1

## Exploring unbinding mechanism of drugs from SERT via molecular dynamics simulation and its implication in antidepressants

Xin-Guan Tan(谭新官), Xue-Feng Liu(刘雪峰), Ming-Hui Pang(庞铭慧), Yu-Qing Wang(王雨晴), and Yun-Jie Zhao(赵蕴杰)
Chin. Phys. B, 2023, 32 (**8**): 088702. DOI: 10.1088/1674-1056/acd687

## Adsorption dynamics of double-stranded DNA on a graphene oxide surface with both large unoxidized and oxidized regions

Mengjiao Wu(吴梦娇), Huishu Ma(马慧姝), Haiping Fang(方海平), Li Yang(阳丽), and Xiaoling Lei(雷晓玲)
Chin. Phys. B, 2023, 32 (**1**): 018701. DOI: 10.1088/1674-1056/ac5c3a

---

# Factors resisting protein adsorption on hydrophilic/hydrophobic self-assembled monolayers terminated with hydrophilic hydroxyl groups

Dangxin Mao(毛党新), Yuan-Yan Wu(吴园燕)[†], and Yusong Tu(涂育松)[‡]

*College of Physics Science and Technology, Yangzhou University, Yangzhou* 225009, *China*

(Received 21 February 2024; revised manuscript received 16 March 2024; accepted manuscript online 3 April 2024)

The hydroxyl-terminated self-assembled monolayer (OH-SAM), as a surface resistant to protein adsorption, exhibits substantial potential in applications such as ship navigation and medical implants, and the appropriate strategies for designing anti-fouling surfaces are crucial. Here, we employ molecular dynamics simulations and alchemical free energy calculations to systematically analyze the factors influencing resistance to protein adsorption on the SAMs terminated with single or double OH groups at three packing densities ($\Sigma = 2.0$ nm$^{-2}$, 4.5 nm$^{-2}$, and 6.5 nm$^{-2}$), respectively. For the first time, we observed that the compactness and order of interfacial water enhance its physical barrier effect, subsequently enhancing the resistance of SAM to protein adsorption. Notably, the spatial hindrance effect of SAM leads to the embedding of protein into SAM, resulting in a lack of resistance of SAM towards protein. Furthermore, the number of hydroxyl groups per unit area of double OH-terminated SAM at $\Sigma = 6.5$ nm$^{-2}$ is approximately 2 to 3 times that of single OH-terminated SAM at $\Sigma = 6.5$ nm$^{-2}$ and 4.5 nm$^{-2}$, consequently yielding a weaker resistance of double OH-terminated SAM towards protein. Meanwhile, due to the structure of SAM itself, i.e., the formation of a nearly perfect ice-like hydrogen bond structure, the SAM exhibits the weakest resistance towards protein. This study will complement and improve the mechanism of OH-SAM resistance to protein adsorption, especially the traditional barrier effect of interfacial water.

**Keywords:** molecular dynamics simulation, self-assembled monolayer, resistance to protein adsorption, hydrogen bond, interfacial water

**PACS:** 87.10.Tf, 64.75.Yz, 87.15.K–, 68.08.–p **DOI:** 10.1088/1674-1056/ad39ca

## 1. Introduction

The adsorption of biological organic macromolecules, such as protein and glycoprotein, onto the underwater substrate is the primary step in the formation of marine biofouling.[1–3] Their adherence to the hull surface will increase surface roughness, consequent navigation resistance and fuel consumption, and more severe acceleration of corrosion,[4] leading to potential safety concerns and economic losses. Therefore, it is crucial for enhancing the anti-fouling properties of surfaces to reduce the probability of life-threatening incidents and operational costs. OH-SAMs are extensively utilized in anti-fouling researches due to their excellent bioinertness and biocompatibility.[5–14]

Experimental and theoretical researchers[5–12,14] revealed that OH-SAMs exhibited unique advantages in resistance to protein/peptide adsorption, which was ascribed to a physical barrier effect formed by a number of hydrogen bonds between interfacial water and OH-SAM with weak charge distribution in the headgroups. This physical barrier effect was traditional mechanistic explanation for OH-SAM resistance to protein adsorption. However, our previous study[15] found that SAM terminated with only hydrophilic OH groups exhibited different hydrophilic and hydrophobic characteristics at different packing densities. For such structures, is the effect of interfacial water on OH-SAM resistance to protein adsorption consistent? Does only interfacial water influence the resistance of OH-SAM to protein adsorption? These issues are necessary to explore for the rational design and precise customization of anti-fouling surfaces. Our recent study[16] has also proposed a new mechanism of resistance to protein adsorption, namely, the structure of SAM itself.

In this study, we utilize molecular dynamics (MD) simulations and alchemical free energy calculations to systematically investigate the factors affecting the resistance of single or double OH-terminated SAM to protein adsorption at three packing densities (2.0 nm$^{-2}$, 4.5 nm$^{-2}$, and 6.5 nm$^{-2}$). The aim is to enrich and improve the mechanism of OH-SAM resistance to protein adsorption, provide directional guidance for the rational design and precise customization of OH-terminated anti-fouling surfaces, and promote their applications in ship navigation and medical implants.[17]

## 2. Models and methods

### 2.1. Models

The SAM consisted of five-carbon long alkyl chains, one end of which was terminated with single or double hydrophilic

[†]Corresponding author. E-mail: yywu@yzu.edu.cn
[‡]Corresponding author. E-mail: ystu@yzu.edu.cn

© 2024 Chinese Physical Society and IOP Publishing Ltd 

OH groups, and the model atoms at the other end were bound to the 111 surface (Fig. 1). The fixation of SAM on the 111 surface was performed to simulate the substrate in experimental conditions. To simplify the procedure, we followed the typical setup described in the literature by fixing model atoms on the 111 surface.[18,19] The chain numbers of SAMs were the same. The packing densities of SAMs were 2.0 $nm^{-2}$, 4.5 $nm^{-2}$, and 6.5 $nm^{-2}$, representing low, medium, and high densities, respectively. The water contact angles for SAMs terminated with two hydrophilic OH groups at the three packing densities were 35.6°, 82°, and 0°,[15] respectively, while those for SAMs terminated with the single OH group were 63.4°, 22°, and 0° (Fig. S3 in supplementary information), respectively. The calculation method for contact angles was consistent with our previous work.[15,19–21] The two OH-terminated SAM at $\Sigma = 4.5$ $nm^{-2}$ with an 82° contact angle was defined as hydrophobic, and the other surfaces of the six systems were classified as hydrophilic.[15,22,23] The crystal structure of protein used in the simulations was taken from the Protein Data Bank (PDB ID: 5DUY).[24] As a mussel protein, it was widely used to study the SAM resistance to protein adsorption[25] due to strong adhesive property.[26–28] The protein was initially placed 6 Å above the SAM. The protein-SAM complex was solvated with SPC/E[29] water molecules. Sodium and chloride ions were added to neutralize the system with a concentration of 0.15 M. The addition of 0.15-M NaCl was implemented to mimic the physiological environment of the human body.[30]

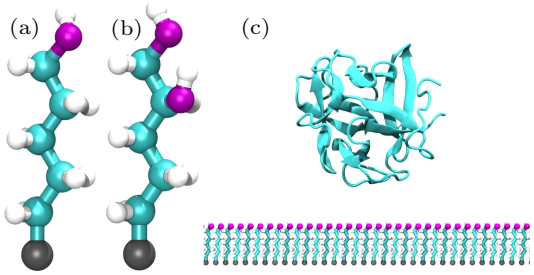



**Fig. 1.** The initial structures of single alkyl chains terminated with an OH group (a) and two OH groups (b), respectively, and the initial structure of protein on the SAM (c). The protein is displayed using the NewCartoon mode, and the alkyl chains are represented in Licorice mode. The rest of the system is omitted for clarity. Color codes: hydroxyl groups, purple and white; main chain, cyan and white; and model atoms, gray.

### 2.2. Equilibrium MD simulations

MD simulations were performed using GROMACS 2019.6 package[31,32] with an OPLS-AA force field.[33] The force field parameters for the OH-SAM were adopted from the built-in parameters of the OPLS force field library, and the entire molecule was electrically neutral. Our previous study has demonstrated that these parameters can produce a reasonable wetting phenomenon.[15] The force field for the protein was generated using the gmx pdb2gmx tool integrated within the GROMACS software package. The particle-mesh Ewald (PME) algorithm[34,35] was used to treat electrostatic interactions with a 1.2-nm cutoff radius. Likewise, a cutoff radius for the van der Waals interaction was 1.2 nm. Newton's equation of motion was integrated using the leap-frog algorithm with a 2-fs integration time step. Periodic boundary conditions were applied in all directions. A velocity rescaling thermostat was used to maintain the temperature at 300 K. All bonds involving hydrogen atoms were constrained using the LINCS algorithm.[36] All systems were equilibrated in the canonical (NVT) ensemble for 300 ns, and the last 20 ns were used for data analysis. The coordinates were saved every 4 ps.

### 2.3. Alchemical free energy calculations

The last structures from MD simulations were used as the starting configurations for further alchemical simulations. The alchemical transformations were divided into two processes, one was the decoupling of protein from the water solution in the solvated protein system, and the other was the decoupling of protein from the solvated protein-SAM complex. The free energy differences ($\Delta G$) were defined as the differences between the free energy changes of the decoupling of protein from the water solution in solvated protein system and those from the solvated complex,[37,38] which was used to characterize the binding affinity of protein to the SAM. A coupling parameter, $\lambda$, ranging from 0 to 1 was introduced to alchemical transformations with an equally spaced value of 0.1 and 21 $\lambda$ windows. It was noticed that $\lambda = 0$ represented the initial state where the electrostatic and van der Waals interactions between protein and the surroundings were fully turned on, while $\lambda = 1$ represented the final state where there was no interaction between protein and the surroundings. The electrostatic interactions were first linearly scaled to 0, and then the van der Waals interactions were turned off using a soft-core potential[39] to avoid singularities. Langevin dynamics[40] were implemented for temperature regulation with a friction coefficient of 2 $ps^{-1}$ and a reference temperature of 300 K in the NVT ensemble. Each $\lambda$ window was equilibrated for 1 ns, and then was sampled for 1 ns. The free energy changes were estimated using the Multistate Bennett Acceptance Ratio (MBAR) method[41] implemented in the pymbar package (https://github.com/choderalab/pymbar).

## 3. Results and discussion

First, the root mean square deviation (RMSD) of the protein backbone on the SAM surface is analyzed (Fig. S1 in the supplementary information). The RMSD results show that the

simulations have converged. The protein has achieved structural equilibrium during the simulation. Meanwhile, the secondary structure analysis provided in Fig. S2 of the supplementary information reveals that the primary secondary structure of protein has been retained, indicating that the native conformation has not been disrupted. We performed statistical analysis on the data from the final 20-ns following simulation convergence. During the equilibration phase, the structural variation of the protein remained minimal with a stable conformation.

The binding affinity of protein to the SAM surface in this study is characterized by the number of hydrogen bonds formed between protein and the SAM, the difference in alchemical free energy, and the contact area between them. The average number of hydrogen bonds is listed in Table 1, which represents the number of the hydrogen bonds among the OH groups of the SAM, between the SAM and interfacial water, and between the SAM and protein at various packing densities. The alchemical free energy differences of protein on single or double OH-terminated SAMs are shown in Fig. 7 at the three packing densities. The contact area of protein on the SAM is shown in Fig. 8, which is calculated using the following formula:[42–44]

$$\text{contact area} = \frac{1}{2}\left(\left(\text{SASA}_{\text{protein}} + \text{SASA}_{\text{surface}}\right) - \text{SASA}_{\text{complex}}\right), \quad (1)$$

where $\text{SASA}_{\text{protein}}$ and $\text{SASA}_{\text{surface}}$ represent the solvent accessible surface area of the isolated protein and the SAM, respectively, and $\text{SASA}_{\text{complex}}$ is that of the protein and SAM complex. A probe of 1.4-Å radius is employed to calculate the individual solvent accessible surface area of the protein, the SAM, and the complex.

### 3.1. The existence of interfacial water

The binding affinity of protein to the SAM surface is influenced by multiple factors, including the well-known physical barrier effect of interfacial water.[14] Due to this barrier effect, the direct adsorption of protein onto the SAM surface is hindered, resulting in OH-SAM exhibiting resistance to protein adsorption. Therefore, we analyzed the RDF of the oxygen atoms in water relative to the topmost OH groups of the SAM to reveal the presence of interfacial water. As shown in Fig. 2, the first peak of RDF reflects the presence of interfacial water near the SAM at the three packing densities. We observed that, irrespective of the single or double OH-terminated SAM systems, the peak of the RDF at $\Sigma = 2.0$ nm$^{-2}$ is consistently the highest, while the RDF at $\Sigma = 4.5_{2\text{OH}}$ nm$^{-2}$ exhibits the lowest peak among all the six systems. It is worth noting that the peak of the RDF at $\Sigma = 6.5_{1\text{OH}}$ nm$^{-2}$ is lower than that at $\Sigma = 4.5_{1\text{OH}}$ nm$^{-2}$, contrary to the order of the peak heights for water density (Fig. 4) at the two packing densities, indicating that interfacial water at $\Sigma = 6.5_{1\text{OH}}$ nm$^{-2}$ is denser. This is analogous to the situation observed at $\Sigma = 2.0$ nm$^{-2}$. The RDF analysis confirms the presence of interfacial water on these SAM surfaces. The barrier effect of interfacial water may have varying degrees of impact on the resistance toward protein. Here, we define the water within 6.5 Å above the topmost OH groups of the SAM as interfacial water.

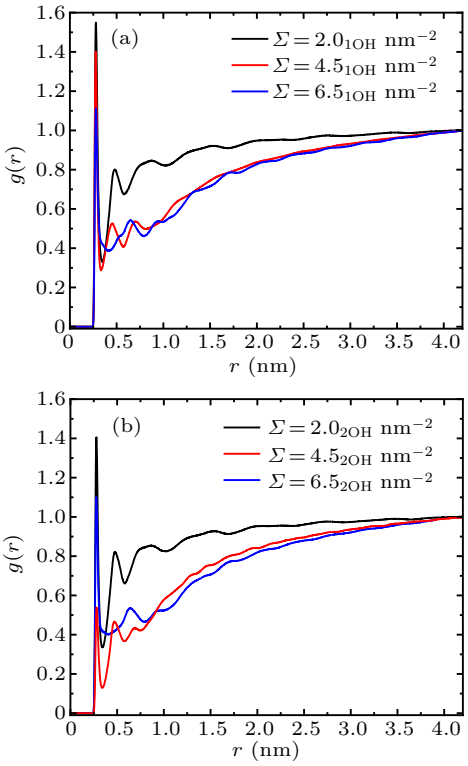



**Fig. 2.** Radial distribution function (RDF) of oxygen atoms in water with respect to the topmost OH groups of the SAM at the three packing densities. Panel (a) corresponds to the case of SAM terminated with a single OH group (denoted by the subscript 1OH, same as below), while panel (b) corresponds to the case of SAM terminated with two OH groups (denoted by the subscript 2OH, same as below). For instance, $\Sigma = 2.0_{1\text{OH}}$ nm$^{-2}$ denotes the system where protein is adsorbed on the SAM terminated with a single OH group with the packing density of 2.0 nm$^{-2}$, and the RDF of oxygen atoms in water corresponds to the packing density of 2.0 nm$^{-2}$.

### 3.2. The effect of compactness and order of interfacial water

As mentioned earlier, the barrier effect of interfacial water reduces protein adsorption on the SAM, and we further found that the resistance of SAM towards protein exhibits variations under the influence of interfacial water at $\Sigma = 4.5_{1\text{OH}}$ nm$^{-2}$ and $6.5_{1\text{OH}}$ nm$^{-2}$, as shown in Fig. 3. It was found that a lower number of hydrogen bonds between protein and the SAM at $\Sigma = 6.5_{1\text{OH}}$ nm$^{-2}$ (Table 1), indicating a weaker binding affinity of protein to the SAM compared to that at $\Sigma = 4.5_{1\text{OH}}$ nm$^{-2}$. Furthermore, the difference in alchemical free energy at $\Sigma = 6.5_{1\text{OH}}$ nm$^{-2}$ is greater compared

to that at $\Sigma = 4.5_{1OH}$ nm$^{-2}$ (Fig. 7), indicating a less stable binding of protein to the SAM at $\Sigma = 6.5_{1OH}$ nm$^{-2}$. This further reflects the weaker binding affinity of protein to the SAM at $\Sigma = 6.5_{1OH}$ nm$^{-2}$. In Fig. 3, we notice that the arrangement of OH groups of SAM at $\Sigma = 6.5_{1OH}$ nm$^{-2}$ is more regular and ordered, consequently leading to a more compact and ordered distribution of interfacial water on the SAM surface. We speculate that this is responsible for the weaker binding affinity of protein to the SAM at $\Sigma = 6.5_{1OH}$ nm$^{-2}$. To demonstrate this, we first analyze the density of water molecules perpendicular to the SAM direction.

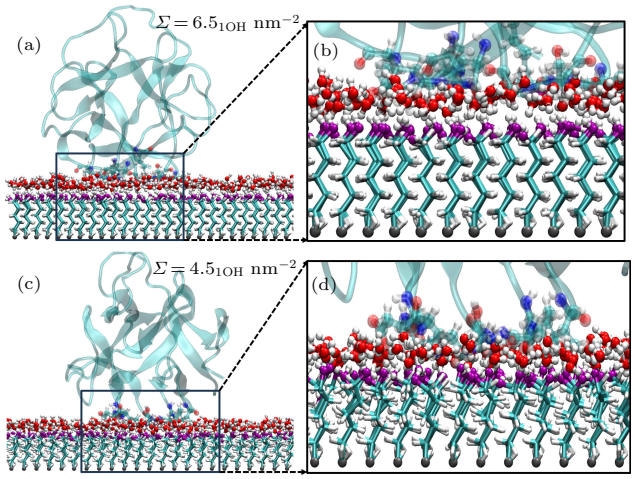



**Fig. 3.** Snapshots of protein adsorption on the SAM at $\Sigma = 6.5_{1OH}$ nm$^{-2}$ [(a), (b)] and $4.5_{1OH}$ nm$^{-2}$ [(c), (d)], with interfacial water highlighted separately. The rest of the system is omitted for clarity. The subfigure represents a partial enlargement of interfacial water on the SAM surface. The proteins are represented using a NewCartoon method with a transparent mode. The protein residues near the SAM surface are displayed in CPK mode. Water molecules are displayed in CPK mode with red and white spheres. The color codes and atomic representations for the rest are the same as those in Fig. 1.

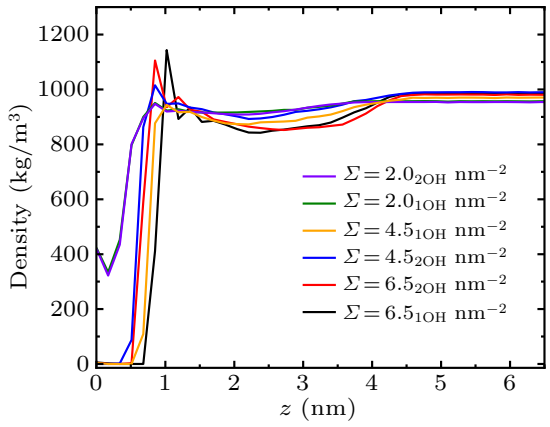



**Fig. 4.** Density distribution of water molecules along the $z$ axis (perpendicular to the SAM surface) at various packing densities. The two density curves at $\Sigma = 2.0$ nm$^{-2}$ exhibit significant overlap.

As shown in Fig. 4, the density of water molecules at $\Sigma = 6.5_{1OH}$ nm$^{-2}$ is significantly higher than that at $\Sigma = 4.5_{1OH}$ nm$^{-2}$, demonstrating the compactness of interfacial water. Further, we analyze the probability of the dipole orientation[45–48] of interfacial water to demonstrate the order of interfacial water at $\Sigma = 6.5_{1OH}$ nm$^{-2}$, as shown in Fig. 5.

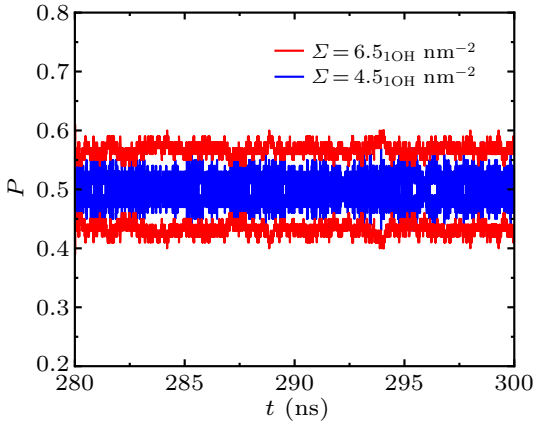



**Fig. 5.** Probability of dipole orientation of interfacial water as a function of time. The red color corresponds to the case of $\Sigma = 6.5_{1OH}$ nm$^{-2}$, while the blue color represents that at $\Sigma = 4.5_{1OH}$ nm$^{-2}$. There are two curves of the same color for each packing density, where the upper curve represents the upward dipole orientation of interfacial water (i.e., the oxygen atom of water facing downward), and the lower curve represents the downward dipole orientation of interfacial water (i.e., the oxygen atom of water facing upward). Here, we define the dipole orientation of interfacial water as an angle less than 90° with the $z$ axis, indicating an upward dipole orientation. Otherwise, downward.

The dipole orientation of interfacial water is defined by the vector connecting the positive charge center of the two hydrogen atoms and the negative charge center of the oxygen atom. The direction is delineated from the negative charge center toward the positive charge center. We calculated the probability of the number of interfacial water molecules with dipole orientation up or down relative to the total number of interfacial water in each frame. Subsequently, we computed the probability values across all time points. Finally, concatenating the probability values at each time point yields the temporal evolution of probability. From Fig. 5, the two blue curves at $\Sigma = 4.5_{1OH}$ nm$^{-2}$ are located between the two red curves at $\Sigma = 6.5_{1OH}$ nm$^{-2}$, indicating that a more disordered dipole orientation of interfacial water caused by the disorder in the distribution of OH groups of SAM at $\Sigma = 4.5_{1OH}$ nm$^{-2}$, i.e., the oxygen atoms of interfacial water exhibit a random distribution, with a mixture of upward and downward orientations. In contrast, the more regular and ordered distribution of OH groups of SAM at $\Sigma = 6.5_{1OH}$ nm$^{-2}$ results in a more ordered dipole orientation of interfacial water compared to that at $\Sigma = 4.5_{1OH}$ nm$^{-2}$. The upper red curve at $\Sigma = 6.5_{1OH}$ nm$^{-2}$ indicates that more oxygen atoms of interfacial water are facing downward to form hydrogen bonds with the upward hydrogen atoms of OH groups of SAM. In Table 1, the higher number of hydrogen bonds (7.27 nm$^{-2}$) between the SAM and interfacial water at $\Sigma = 6.5_{1OH}$ nm$^{-2}$ further confirms a more favorable structure arrangement for hydrogen bond formation between the SAM and interfacial water compared to that (6.19 nm$^{-2}$) at $\Sigma = 4.5_{1OH}$ nm$^{-2}$. Therefore, the compactness and order of interfacial water enhance its barrier effect, thereby enhancing resistance to protein adsorption on the SAM.

**Table 1.** Hydrogen bond number analysis.

| System[a] | $\Sigma$ (nm$^{-2}$) | SAM–SAM | SAM–water | SAM–protein |
|---|---|---|---|---|
| 1OH | 2.0 | 0.14 | 0.92 | 4.39 |
| | 4.5 | 0.85 | 6.19 | 3.92 |
| | 6.5 | 1.32 | 7.27 | 3.35 |
| 2OH | 2.0 | 0.30 | 1.71 | 5.82 |
| | 4.5 | 8.02 | 2.85 | 0.64 |
| | 6.5 | 2.08 | 6.98 | 5.56 |

[a] The number of OH groups in the alkyl chain. 1OH represents the single OH-terminated SAM system, while 2OH represents the double OH-terminated SAM system (same as below).

### 3.3. The spatial hindrance effect of SAM

The binding affinity of protein to the SAM surface is also influenced by the spatial hindrance effect of SAM. From Fig. 6, it can be observed that the protein is embedded into SAM, which can be primarily ascribed to the spatial hindrance effect of SAM at $\Sigma = 2.0_{2OH}$ nm$^{-2}$.

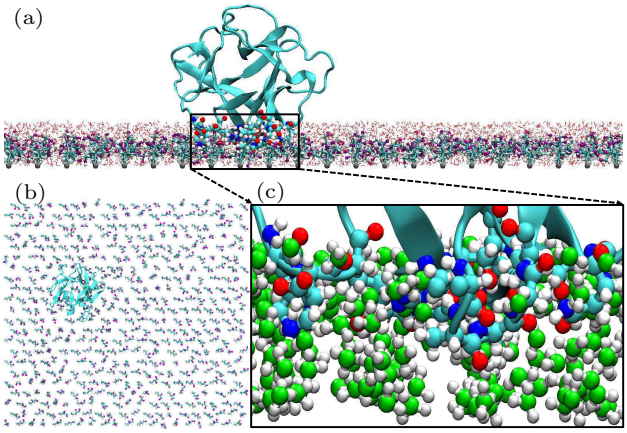



**Fig. 6.** (a) A side view of protein embedded into SAM at $\Sigma = 2.0_{2OH}$ nm$^{-2}$. The interfacial water and the water penetrating into SAM are highlighted separately in a linear mode. The protein is represented in a NewCartoon mode, while the protein residues near the SAM surface are displayed using the CPK representation. The rest of the system is omitted for clarity. The color codes and atomic representations for the rest are the same as those in Fig. 1. (b) A top view of protein embedded into SAM. Water molecules are also omitted for clarity. (c) A magnified view of protein embedded into SAM. Water molecules are represented by green and white spheres.

Here, the spatial hindrance effect of SAM indicates that the spacing between the molecular chains constituting SAM at low packing densities is too large, and the SAM and interfacial water are unable to effectively impede protein adsorption. The protein encounters a low energy barrier, leading to its easy insertion into the interstices of SAM. Hence, the protein is embedded into SAM and tightly binding to SAM under the influence of the spatial hindrance effect. Moreover, the conformation of SAM differs between states of resistance (medium to high packing densities) and lack of resistance (low packing density). The SAM at low packing density displays significant conformational flexibility, with the molecular chains in a collapsed state. While the SAM exhibits good resistance at medium to high packing densities where the conformation of SAM becomes relatively rigid and ordered, compared to that of low packing density. We also noted that the spatial hindrance effect leads to the lowest number of hydrogen bonds among OH groups of the SAM (see Table 1, 0.14 for $\Sigma = 2.0_{1OH}$ nm$^{-2}$ and 0.30 for $\Sigma = 2.0_{2OH}$ nm$^{-2}$) within the three packing densities, indicating the minimal impact of the structure of SAM itself (detailed analysis in Subsection 3.5) on resistance towards protein. Although double hydroxyl modification increases the number of hydroxyl groups per unit area of SAM, excessive distance between molecular chains hinders the formation of hydrogen bonds among hydroxyl groups of SAM. Therefore, the increased number of hydroxyl groups per unit area of SAM has not led to a greater formation of hydrogen bonds among hydroxyl groups of SAM. Furthermore, the spatial hindrance effect also results in the lowest number of hydrogen bonds between SAM and interfacial water at $\Sigma = 2.0$ nm$^{-2}$ (see Table 1, 0.92 for $\Sigma = 2.0_{1OH}$ nm$^{-2}$ and 1.71 for $\Sigma = 2.0_{2OH}$ nm$^{-2}$), indicating the weakest barrier effect of interfacial water on resistance towards protein. As shown in Fig. 6, we notice that the spatial hindrance effect allows water penetration into SAM, which can be reflected by the non-zero minimum density at $\Sigma = 2.0$ nm$^{-2}$ as shown in Fig. 4. Furthermore, the RDF at $\Sigma = 2.0$ nm$^{-2}$ exhibits the highest peak, indicating a substantial accumulation of water molecules near the SAM. Also, the relatively low density of water in Fig. 4 further confirms the weak barrier effect of interfacial water, which is consistent with the lowest number of hydrogen bonds between the SAM and interfacial water at $\Sigma = 2.0$ nm$^{-2}$. Therefore, protein can easily displace water molecules and subsequently embed itself into SAM. At this time, the number of hydrogen bonds (see Table 1, 4.39 for $\Sigma = 2.0_{1OH}$ nm$^{-2}$ and 5.82 for $\Sigma = 2.0_{2OH}$ nm$^{-2}$) between the protein and SAM is the largest, indicating the strongest binding affinity of protein to the SAM. We observed that the difference in alchemical free energy of protein on the SAM surface was minimized (as shown in Fig. 7) at $\Sigma = 2.0$ nm$^{-2}$, corresponding to the largest contact area between protein and the SAM (as shown in Fig. 8). These findings further confirm the strongest binding affinity of protein to the SAM. Hence, the protein is embedded into the SAM under the influence of the spatial hindrance effect, and the SAM exhibits a lack of the resistance towards the protein. The simulation snapshots at $\Sigma = 2.0_{1OH}$ nm$^{-2}$ are provided in Fig. S4 of supplementary information.

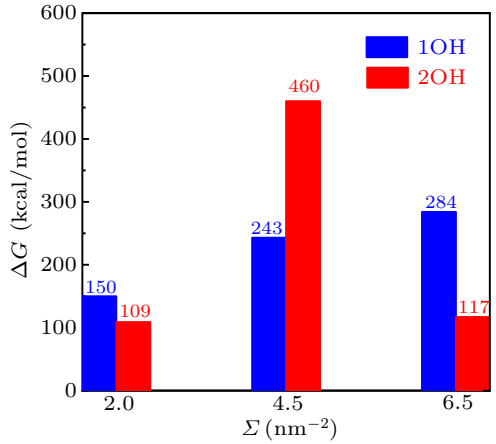



**Fig. 7.** Free energy differences of proteins on single or double OH-terminated SAMs at various packing densities. The blue color represents the free energy difference for the single OH-terminated SAM system, while the red color represents the free energy difference for the double OH-terminated SAM system. The data are divided into three groups, i.e., the first two are grouped together, representing the free energy difference at $\Sigma = 2.0$ nm$^{-2}$. The middle two are grouped together, representing the free energy difference at $\Sigma = 4.5$ nm$^{-2}$. The last two are grouped together, representing the free energy difference at $\Sigma = 6.5$ nm$^{-2}$.

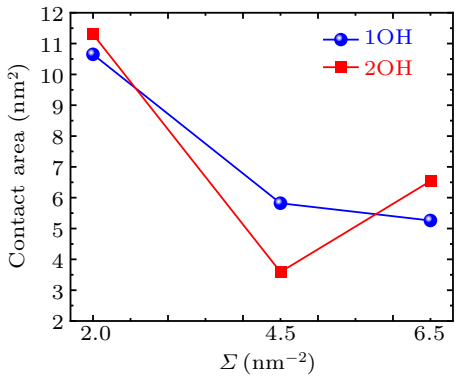



**Fig. 8.** The average contact area of proteins on single or double OH-terminated SAM surfaces at the three packing densities. The blue color represents the contact area of protein on the single OH-terminated SAM, while the red color represents the contact area of protein on the double OH-terminated SAM.

### 3.4. The effect of the number of hydroxyl groups per unit area of SAM

We observed that the resistance of SAM towards protein is also modulated by the number of hydroxyl groups per unit area of SAM. As shown in Table 1, the number of hydrogen bonds between protein and the SAM at $\Sigma = 6.5_{2OH}$ nm$^{-2}$ (5.56) is greater than that at $\Sigma = 6.5_{1OH}$ nm$^{-2}$ (3.35) and $\Sigma = 4.5_{1OH}$ nm$^{-2}$ (3.92), indicating a weaker resistance of SAM towards protein at $\Sigma = 6.5_{2OH}$ nm$^{-2}$. It can be seen that the number of hydrogen bonds (0.85 at $\Sigma = 4.5_{1OH}$ nm$^{-2}$, 1.32 at $\Sigma = 6.5_{1OH}$ nm$^{-2}$, and 2.08 at $\Sigma = 6.5_{2OH}$ nm$^{-2}$) formed among OH groups of SAM in the three cases is significantly lower than the number of hydrogen bonds (6.19 at $\Sigma = 4.5_{1OH}$ nm$^{-2}$, 7.27 at $\Sigma = 6.5_{1OH}$ nm$^{-2}$, and 6.98 at $\Sigma = 6.5_{2OH}$ nm$^{-2}$) formed between SAM and interfacial water, indicating that the barrier effect of interfacial water plays a dominant role in the resistance of SAM towards protein. We also observed that the dense distance between molecular chains at $\Sigma = 6.5_{2OH}$ nm$^{-2}$ disrupts the favorable condition for hydrogen bond formation among hydroxyl groups of SAM, resulting in a rapid decrease in the number of hydrogen bonds (2.85) formed among hydroxyl groups of SAM, compared to that of $\Sigma = 4.5_{2OH}$ nm$^{-2}$. Therefore, the hydroxyl groups of SAM offer more available hydrogen bonding sites for binding with protein. At this moment, the hydroxyl groups of SAM exhibit a stronger inclination to form hydrogen bonds with protein. Furthermore, we notice that the number of OH groups per unit area of double OH-terminated SAM differs significantly from that of single OH-terminated SAM, i.e., the number of OH groups (12.95) per unit area of SAM at $\Sigma = 6.5_{2OH}$ nm$^{-2}$ is approximately 2 to 3 times that at $\Sigma = 6.5_{1OH}$ nm$^{-2}$ (6.56) and $\Sigma = 4.5_{1OH}$ nm$^{-2}$ (4.59), as shown in Table 2. This advantage further amplifies the binding between hydroxyl groups of SAM and protein. Consequently, the SAM at $\Sigma = 6.5_{2OH}$ nm$^{-2}$ can provide more hydrogen bonding sites to form hydrogen bonds with protein, and result in the highest number of hydrogen bonds formed between the SAM and protein in the three cases, indicating that the SAM at $\Sigma = 6.5_{2OH}$ nm$^{-2}$ exhibits the weakest resistance to protein adsorption. Furthermore, it can be seen in Fig. 7 that the alchemical free energy difference of protein adsorption on the SAM at $\Sigma = 6.5_{2OH}$ nm$^{-2}$ is lower than that at the other two packing densities, further confirming the weakest resistance of SAM at $\Sigma = 6.5_{2OH}$ nm$^{-2}$ to protein adsorption in the three cases. Therefore, the number of hydroxyl groups per unit area of SAM can significantly impact the resistance of SAM to protein adsorption.

**Table 2.** The number of OH groups per unit area of SAM.

| System | $\Sigma$ (nm$^{-2}$) | $N_{OH}$ (nm$^{-2}$)[a] |
|---|---|---|
| 1OH | 4.5 | 4.59 |
| | 6.5 | 6.56 |
| 2OH | 6.5 | 12.95 |

[a]The number of OH groups per unit area of SAM.

### 3.5. The impact of the structure of SAM itself

We further observed that the resistance of SAM towards protein is also affected by the structure of SAM itself. As shown in Table 1, the number of hydrogen bonds (0.64) between protein and the SAM at $\Sigma = 4.5_{2OH}$ nm$^{-2}$ (the simulation snapshot is provided in Fig. S5 of supplementary information) is the lowest among all systems, indicating the strongest resistance of SAM to protein adsorption. We noticed that the number of hydrogen bonds (2.85) between the SAM and interfacial water at $\Sigma = 4.5_{2OH}$ nm$^{-2}$ is the lowest at all medium and high packing densities, while the number of hydrogen bonds (8.02) among OH groups of SAM is the highest. This

trend at $\Sigma = 4.5_{2OH}$ nm$^{-2}$ is opposite to the corresponding number of hydrogen bonds (i.e., SAM–water, SAM–SAM) at other medium and high packing densities, indicating that the effect of the structure of SAM itself on resistance to protein adsorption is significantly greater than that of interfacial water. We noted that although there is an increased number of hydroxyl groups per unit area of SAM at $\Sigma = 4.5_{2OH}$ nm$^{-2}$, the majority of hydrogen bonding sites provided by them are predominantly utilized for the formation of hydrogen bonds among hydroxyl groups of SAM. Upon careful examination of the SAM structure, it is found that a nearly perfect ice-like hydrogen bonding structure (the simulation snapshot is provided in Fig. S6 of supplementary information) is formed among OH groups of SAM at $\Sigma = 4.5_{2OH}$ nm$^{-2}$. Further, the hydrogen bonding sites among OH groups of SAM are close to saturation, leaving only a small number of hydrogen bond sites available for binding with protein. This results in the lowest number of hydrogen bonds formed between the SAM and protein, corresponding to the largest difference in the alchemical free energy of protein on the SAM (Fig. 7) and the smallest contact area between them (Fig. 8). Therefore, the SAM exhibits the strongest resistance to protein adsorption due to the structure of SAM itself.

## 4. Conclusions

In this study, we have utilized MD simulations and alchemical free energy calculations to systematically investigate the factors influencing the resistance to protein adsorption on single or double OH-terminated SAMs at various packing densities. The results show that four factors play a significant role in the resistance of SAM to protein adsorption, namely, the compactness and order of interfacial water, the spatial hindrance effect of SAM, the number of hydroxyl groups per unit area of SAM, and the structure of SAM itself.

For the first time, we found that interfacial water at $\Sigma = 6.5_{1OH}$ nm$^{-2}$ is denser and more ordered compared to that at $\Sigma = 4.5_{1OH}$ nm$^{-2}$, resulting in a lower number of hydrogen bonds between the SAM and protein at $\Sigma = 6.5_{1OH}$ nm$^{-2}$. Therefore, the compactness and order of interfacial water enhance its barrier effect, thereby enhancing the resistance of SAM towards protein. We further found that the protein is embedded into SAM due to the spatial hindrance effect of SAM at $\Sigma = 2.0$ nm$^{-2}$, corresponding to the maximum number of hydrogen bonds between protein and the SAM, and the SAM exhibits a lack of resistance towards protein. We also found that the number of hydroxyl groups per unit area of SAM at $\Sigma = 6.5_{2OH}$ nm$^{-2}$ is approximately 2 to 3 times that at $\Sigma = 6.5_{1OH}$ nm$^{-2}$ and $\Sigma = 4.5_{1OH}$ nm$^{-2}$. The SAM at $\Sigma = 6.5_{2OH}$ nm$^{-2}$ can provide more hydrogen bonding sites to form hydrogen bonds with protein, resulting in a weaker resistance of SAM to protein adsorption. Therefore, the number of OH groups per unit area of SAM can significantly affect the resistance of SAM towards protein. Meanwhile, we also found that the structure of SAM itself, i.e., the formation of a nearly perfect ice-like hydrogen bond structure results in the least number of hydrogen bonds formed between the SAM and protein, and the SAM exhibits the strongest resistance towards protein.

Our findings enrich and improve the understanding of the mechanism underlying the resistance of OH-SAM to protein adsorption, particularly the traditional barrier effect of interfacial water. These findings are of great significance for the rational design and precise customization of OH-terminated anti-fouling surfaces, with potential applications in ship navigation and medical implants.

## Acknowledgements

Project supported by the National Natural Science Foundation of China (Grants No. 12075201), the Science and Technology Planning Project of Jiangsu Province, China (Grant No. BK20201428), the Postgraduate Research & Practice Innovation Program of Jiangsu Province, China (Grant No. KYCX21_3193), and the Special Program for Applied Research on Supercomputation of the NSFC–Guangdong Joint Fund (the second phase).

## References

[1] Jain A and Bhosle N B 2009 *Biofouling* **25** 13
[2] Ma C, Yang H, Zhou X, Wu B and Zhang G 2012 *Colloid Surface B* **100** 31
[3] Li X, Li S, Huang X, Chen Y, Cheng J and Zhan A 2021 *Mar. Environ. Res.* **170** 105409
[4] de Carvalho C C C R 2018 *Front. Mar. Sci.* **5** 126
[5] Martins M C L, Fonseca C, Barbosa M A and Ratner B D 2003 *Biomaterials* **24** 3697
[6] Choi S, Yang Y and Chae J 2008 *Biosens. Bioelectron.* **24** 893
[7] Guo J, Zhang P, Chen Y, Shen Y, Hu X, Yan P, Yang J, Fang F, Li C, Gao X and Wang G 2015 *Chem. Eng. J.* **279** 516
[8] Miyake T, Tanii T, Kato K, Zako T, Funatsu T and Ohdomari I 2007 *Nanotechnology* **18** 305304
[9] Huang S, Hou Q, Guo D, Yang H, Chen T, Liu F, Hu G, Zhang M, Zhang J and Wang J 2017 *RSC. Adv.* **7** 39530
[10] Zhao J, Wang Q, Liang G and Zheng J 2011 *Langmuir* **27** 14876
[11] Wang Q, Zhao C, Zhao J, Wang J, Yang J C, Yu X and Zheng J 2010 *Langmuir* **26** 3308
[12] Peng C, Liu J, Zhao D and Zhou J 2014 *Langmuir* **30** 11401
[13] Li M, Xie Y, Lin F R, Li Z, Yang S and Jen A K 2023 *Innovation* **4** 100369
[14] Wang Q, Zhao J, Yu X, Zhao C, Li L and Zheng J 2010 *Langmuir* **26** 12722
[15] Mao D, Wang X, Wu Y, Gu Z, Wang C and Tu Y 2021 *Nanoscale* **13** 19604
[16] Mao D, Wu Y Y and Tu Y 2023 *Phys. Chem. Chem. Phys.* **25** 21376
[17] Zhang Z and Dai J 2024 *Innovation* **5** 100595
[18] Shenogina N, Godawat R, Keblinski P and Garde S 2009 *Phys. Rev. Lett.* **102** 156101
[19] Guo P, Tu Y, Yang J, Wang C, Sheng N and Fang H 2015 *Phys. Rev. Lett.* **115** 186101
[20] Chen Z, Qi C, Teng X, Zhou B and Wang C 2021 *Commun. Theor. Phys.* **73** 115501

[21] Qu M, Huang G, Liu X, Nie X, Qi C, Wang H, Hu J, Fang H, Gao Y, Liu W T, Francisco J S and Wang C 2022 *Chem. Sci.* **13** 10546
[22] Miao W, Tian Y and Jiang L 2022 *Acc. Chem. Res.* **55** 1467
[23] Tian Y and Jiang L 2013 *Nat. Mater.* **12** 291
[24] Jakob M, Lubkowski J, O'Keefe B R and Wlodawer A 2015 *Acta Crystallogr F.* **71** 1429
[25] He C, Zhang H, Lin C, Wang L and Yuan S 2017 *Chem. Phys. Lett.* **676** 144
[26] Fan X, Fang Y, Zhou W, Yan L, Xu Y, Zhu H and Liu H 2021 *Mater. Horiz.* **8** 997
[27] Ou X, Xue B, Lao Y, Wutthinitikornkit Y, Tian R, Zou A, Yang L, Wang W, Cao Y and Li J 2020 *Sci. Adv.* **6** eabb7620
[28] Xuan Z, Li J, Liu Q, Yi F, Wang S and Lu W 2021 *Innovation* **2** 100081
[29] Berendsen H J C, Grigera J R and Straatsma T P 1987 *J. Phys. Chem.* **91** 6269
[30] Azam F, Eid E E M and Almutairi A 2021 *J. Mol. Struct.* **1246** 131124
[31] Van Der Spoel D, Lindahl E, Hess B, Groenhof G, Mark A E and Berendsen H J 2005 *J. Comput. Chem.* **26** 1701
[32] Abraham M J, Murtola T, Schulz R, Páll S, Smith J C, Hess B and Lindahl E 2015 *Software X* **1–2** 19
[33] Jorgensen W L, Maxwell D S and Tirado-Rives J 1996 *J. Am. Chem. Soc.* **118** 11225
[34] Darden T, York D and Pedersen L 1993 *J. Chem. Phys.* **98** 10089
[35] Essmann U, Perera L, Berkowitz M L, Darden T, Lee H and Pedersen L G 1995 *J. Chem. Phys.* **103** 8577
[36] Hess B, Bekker H, Berendsen H J C and Fraaije J G E M 1997 *J. Comput. Chem.* **18** 1463
[37] Aldeghi M, Heifetz A, Bodkin M J, Knapp S and Biggin P C 2016 *Chem. Sci.* **7** 207
[38] Mobley D L, Chodera J D and Dill K A 2006 *J. Chem. Phys.* **125** 084902
[39] Beutler T C, Mark A E, van Schaik R C, Gerber P R and van Gunsteren W F 1994 *Chem. Phys. Lett.* **222** 529
[40] Pastor R W, Brooks B R and Szabo A 2006 *Mol. Phys.* **65** 1409
[41] Shirts M R and Chodera J D 2008 *J. Chem. Phys.* **129** 124105
[42] Luan B, Huynh T, Zhao L and Zhou R 2015 *ACS Nano* **9** 663
[43] Ye R, Song W, Feng M and Zhou R 2021 *Nanoscale* **13** 19255
[44] Feng M, Kang H, Yang Z, Luan B and Zhou R 2016 *J. Chem. Phys.* **144** 225102
[45] Mao D, Wang X, Zhou G, Zeng S, Chen L, Chen J and Dai C 2019 *Chin. Phys. Lett.* **36** 103101
[46] Tu Y, Lu H, Zhang Y, Huynh T and Zhou R 2013 *J. Chem. Phys.* **138** 015104
[47] Tu Y, Zhou R and Fang H 2010 *Nanoscale* **2** 1976
[48] Tu Y, Xiu P, Wan R, Hu J, Zhou R and Fang H 2009 *Proc. Natl. Acad. Sci. USA* **106** 18120